

STRAIN AND TEMPERATURE MEASUREMENTS FROM THE SNS* MERCURY TARGET VESSEL DURING HIGH INTENSITY BEAM PULSES

W. Blokland[†], Y. Liu, B. Riemer, M. Wendel, D. Winder, Oak Ridge National Laboratory,
Oak Ridge, USA

Abstract

To better understand the mechanical impact of the proton beam on the lifetime on Spallation Neutron Source (SNS*) mercury-filled, stainless steel targets, these targets are now instrumented with optical and metal strain sensors, temperature sensors, and accelerometers. The strain and temperature sensors are placed inside the target vessel, between the water shroud and mercury vessel, while the accelerometers are placed outside on the target mount and on the mercury return line. We now have data from four targets. The first instrumented target used regular multimode optical sensors, while later targets have used radhard multimode sensors. We are also developing super-radhard single-mode optical strain sensors to get data further into the production cycle. In this paper, we describe the data-acquisition system, compare the measured strain to the simulated strain for the different targets, estimate the survivable radiation level for each type of sensor, and discuss the implications of the results on the lifetime of the target.

INTRODUCTION

At SNS, a proton beam of up to 1.4 MW hits a mercury-filled target to produce neutrons for material research. A predictable target life-time would allow us to schedule the replacements without unexpected downtime interrupting users' experiments. A longer life-time will reduce costs and require fewer scheduled beam outages to replace a target per year.

Target Lifetime

The lifetime of the target is limited by the damage due to mercury cavitation damage, the administrative radiation damage limit to the steel vessel, and fatigue. A failed target is detected by the leaking mercury flowing from the inner vessel to the interstitial space inside the water shroud and activating the leak detectors. Failures have resulted in lower than expected target lifetimes.

To better understand the impact of the proton beam on the target lifetime, we have begun installing strain sensors on the mercury vessel wall on all new targets, starting with T13, see [1]. The sensors must be installed on the inner

mercury vessel and not on the outside of the water shroud, because the mechanical connection between the two is in the back at the target mount and thus the shroud would not give us representative measurements relating to strain in the mercury vessel, see Fig. 1.

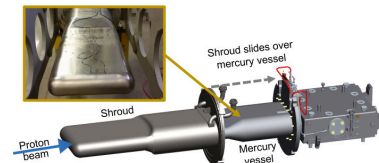


Figure 1: Strain sensors on the mercury vessel.

Measurement Goals

The goals of the strain measurements are to verify the accuracy of the single pulse simulations, to determine if there are any resonances when pulses repeat at 60 Hz, to measure the effect of (future) mitigating mechanisms, such as gas bubble injection, and to detect possible internal failures, such as internal baffle cracks inside the mercury vessel. While the Post-Irradiation Examination (PIE) has the final word on the effectiveness of the mitigation methods on the cavitation damage, this can only be done after a target has been used, and thus only the integrated effect can be seen. The sensors can instantly see the strain while a mitigation method, such as the helium bubble injection, can be turned on and off pulse by pulse.

INSTRUMENTATION

Strain Sensors

There are several environmental considerations for the strain sensors: the radiation levels damaging the sensors, the effect of the electrical noise on the sensors, and the possible negative effect of the sensors on the vessel leak detectors. If our sensor could possibly either short out or coat the wire leak detectors with an insulator, we could no longer reliably determine a leak in the target.

A signal bandwidth of about 50 kHz or higher is preferred and a sensitivity of 10 to 500 microstrain is required, based on target strain experiments at LANL, see [2]. Therefore, we selected strain sensors based on multi-mode optical sensors from FISO. Meanwhile, single-mode fiber strain sensors have been developed to improve the sensor lifetime and measurement bandwidth, see [3].

Other Sensors

Table 1 shows the number and type of sensors installed on the instrumented targets. While the metal strain sensors were not successful for the LANL experiment, we did want to try these sensors and measure their noise levels and radiation hardness. They are installed starting with target T15

*This manuscript has been authored by UT-Battelle, LLC, under Contract No. DE-AC0500OR22725 with the U.S. Department of Energy. This research was supported by the DOE Office of Science, Basic Energy Science, and Scientific User Facilities. The United States Government retains and the publisher, by accepting the article for publication, acknowledges that the United States Government retains a non-exclusive, paid-up, irrevocable, world-wide license to publish or reproduce the published form of this manuscript, or allow others to do so, for the United States Government purposes. The Department of Energy will provide public access to these results of federally sponsored research in accordance with the DOE Public Access Plan (<http://energy.gov/downloads/doe-public-access-plan>)

[†] blokland@ornl.gov

but in only the back on the target so they cannot affect the leak detectors. We have also installed thermo-couples in the back of the target. Two accelerometers are installed outside the target: on the target mount block and on the mercury return line. They will last the entire life of a target but their data have not shown yet a correlation with possible target failures.

Table 1: Instrumented Targets

Target	MM Strain	SM Strain	Thermo couple	Metal strain	Accelerometer
T13 [†]	4/8	-	-	-	2/2
T14 [†]	3/8	2/4	2/2	-	2/2
T15 [†]	9/12	3/4	2/2	1/2	2/2
T16 [*]	10/12	3/4	2/2	2/2	2/2

[†]Standard target, ^{*}jet-flow target
x/y: number of sensors working/installed

Data-acquisition

The data acquisition system, which is based on LabVIEW software, has increased in capabilities over the four instrumented targets. We now have two independent PXI-based data-acquisition crates: one for the multimode strain sensors, accelerometers, metal strain gauges, thermocouples and accelerator data, and one system for the single mode sensors. These systems will be merged in the future, once the single-mode system has been finalized.

MEASUREMENTS

Strain Measurements among Different Targets

The first three instrumented targets are standard types, while the fourth target is the jet-flow type. The jet-flow target has different internal structure and thus has a different strain response, and we cannot expect identical responses to the standard-type target. As not all sensors were working on all targets, we don't have a single location with overlap of sensors between all three standard targets, but can compare between two targets. Figure 2 shows the comparison of strain sensor 2, located on the front of the target, for T13 and T15, as the T14 sensor was not functioning. It shows a factor of two difference for that sensor, while the simulation results agree with target T15. We surmise that this is due to a bad glue bond of the sensor to the target.

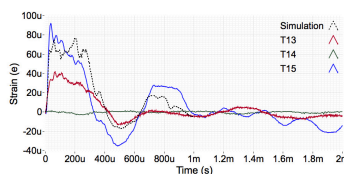


Figure 2: Comparison of sensor 2 (front).

Figure 3 shows the strain signals from the three standard targets. The signal from T14 is suspect as it only shows positive signals. The initial amplitudes vary from 12 to 17 microstrain, and we do see good similarities in the waveform shape.

In general, we see reasonable agreement in the shapes of the waveforms and amplitude variations within a factor of two, and closer if we exclude possible bad glue bonds. We do expect to see some signal variations, due to the variation in placing the sensors on each target.

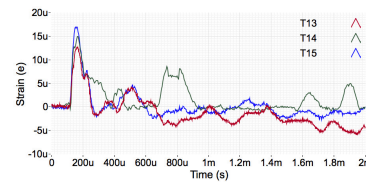


Figure 3: Comparison of sensor 4 (back).

At some locations, for example, towards the back and in the middle, which is near an internal baffle, we do see significant echoes in the strain. This is true for both style targets, as shown in Fig. 4. We have not yet compared this to the simulation results because, at this point, the simulation data only goes out for 1 ms.

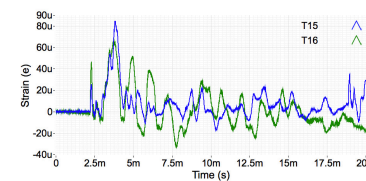


Figure 4: Sensor 3 (middle) from T15 and T16 compared.

As shown before in [1] for T13 and T14, we do not see resonance for consecutive pulses in T15 and T16 either, excluding this as a target failure source, see Fig. 5.

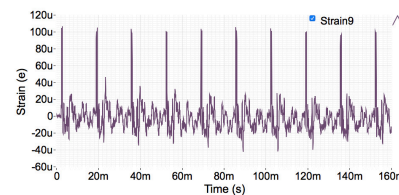


Figure 5: The strain from T16 sensor 9 (front corner), 10 20.8 uC pulses in a row, shows no signal build-up.

Figure 6 shows the signals from the metal strain gauges in T16. The signals are processed to remove 60 Hz noise and are small, as expected, because of their location far in the back. The bandwidth, at most 5 kHz, and noise levels compare unfavorably to the strain sensors.

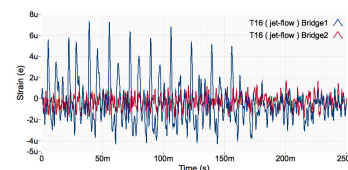


Figure 6: The strain measured by the metal strain gauges (far in the back) with 10 pulses at 3.4 uC.

Figure 7 shows the response of Strain C, a single mode sensor, compared to strain 9, a multi-mode sensor, and the simulation. The two sensors are symmetrically placed on

opposite front corners and should have a very similar response. We see that in amplitude, they are very similar but differ somewhat in shape. As we install more single-mode sensors, we expect to get more comparisons to help evaluate why there are differences.

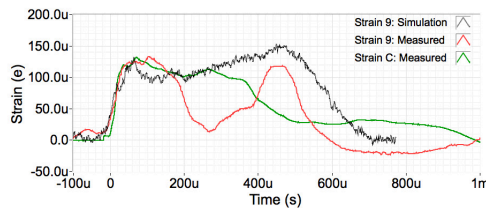


Figure 7: Comparison with single-mode sensor.

Radiation Resistance

The initial multi-mode strain sensors used on T13 were regular multi-mode sensors and these lasted only up to 88 beam pulses. The next targets were instrumented with sensors built with high OH content multimode fibers and single-mode sensors which lasted much longer. The multi-mode sensors can last up to about 3.5 GRads (data from T14) while single-mode sensors can last up to 120 GRads (data from T15). For a sensor location up front, this is almost 4 days at 1MW beam power for the single-mode sensor but less than 4 hours for a multi-mode sensor. Single-mode sensors in the back could last an entire target lifetime.

The epoxy glue, Stycast 2850FT, that bonds the sensor to the stainless-steel wall is also sensitive to radiation. Figure 8 shows the results of trying to pry loose (with remote manipulators) the different glue spots on a used target, see [4]. While this is not an accurate test of the bond between the sensor and the vessel, it does give us an idea on whether we could have glue failures. Comparing the 120 GRad survival dose of a single-mode sensor to data in Fig. 8, we see that glue drops are getting loose before the sensor could be dead. Indeed, we have seen single-mode sensors fail before the radiation attenuation of the optical fiber was beyond the optical processor’s sensitivity.

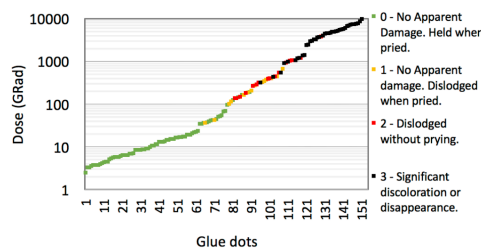


Figure 8. Radiation damage to the epoxy glue.

Measurements Compared to Simulations

Excluding possible bad sensors or bad glue bonds, we see good agreements between the measurements and simulations, described in [5], but better in the front than in the back. For T16, the measured amplitudes were within 20%, except for sensor 10 (side of target), which had a factor of 2.5 difference. The simulation also predicts the arrival times of the main strain signal correctly for different sensor

locations, see Fig. 9. It shows that both the measured and simulated signals at the front corner see the strain signal later than a sensor located in the back. This is due to how the shockwave propagates through the structure.

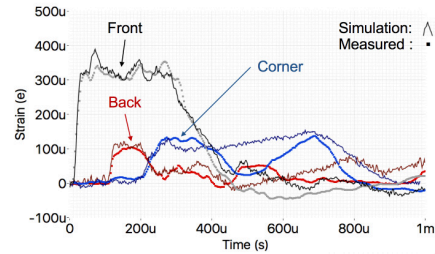


Figure 9: Arrival times of the simulated and measured strain waveforms versus the sensor locations.

Temperature Measurements

For T15, we verified the linearity of the temperature response versus the amount of beam charge, see Fig. 10. A pulse train of 300 pulses each of the indicated charge was used to generate the temperature increase. This is only valid for short bursts of beam, because the cooling process will start reducing the temperature increase over longer time scales.

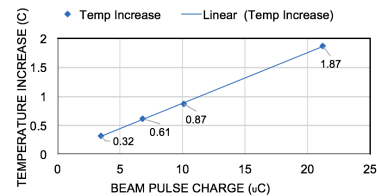


Figure 10: Increased beam power gives a linear increase in temperature.

SUMMARY

Especially for T16, excluding one sensor, the simulation matched the measurements very well, increasing our trust in the simulation and the installation of the sensors. We have not found any structural resonance problems, meaning that the focus will be on the mitigation methods.

Differences between simulations and measurements are being investigated as potential keys to future simulation improvement. The measurements allow us to proceed with more confidence in designing and building longer lasting targets using the simulations as a guiding tool.

We do plan to evaluate different glues so that we can have the sensors reliably attached for high radiation doses.

We are ready to test mitigation methods for future targets, such as gas injection and jet-flow, and the strain sensors will be critical to evaluating the mitigation effectiveness as no simulation exist yet to simulate the helium gas injection process.

ACKNOWLEDGMENT

The authors wish to acknowledge the installation of the sensors by Bob Sangrey and the radiation calculations by Wei Lu.

REFERENCES

- [1] W. Blokland *et al.*, “Measurements of beam pulse induced mechanical strain inside the SNS* target module”, Proceeding of the High Brightness Workshop, Malmö, Sweden, July 3-8, 2016, paper THAM2Y01, pp. 532-7.
- [2] B. Riemer *et al.*, “Small gas bubble experiment for mitigation of cavitation damage and pressure waves in short-pulse mercury spallation targets”, Journal of Nuclear Materials, Volume 450 (2014) 192.
- [3] Y. Liu *et al.*, “Radiation-Resistant Fiber Optic Strain Sensors for SNS Target Instrumentation”, in Proc. 7th International Particle Accelerator Conference (IPAC'16), Busan, Korea, May 2016, paper MOPMR055, pp. 371-373.
- [4] D. Winder *et al.*, “Target Systems, Irradiation Performance of Epoxy on Target 13 (MTX-009),” ORNL 106010101-TR0031, R00, 2016.
- [5] B. Riemer, “Benchmarking dynamic strain predictions of pulsed mercury spallation target vessels”, Journal of Nuclear Materials, Volume 343, 1 August 2005, P 81–91, doi:10.1016/j.jnucmat.2005.01.026.